



Characterisation of white etching crack damage in wind turbine gearbox bearings



T. Bruce, E. Rounding, H. Long*, R.S. Dwyer-Joyce

Leonardo Centre for Tribology, Department of Mechanical Engineering, The University of Sheffield, United Kingdom

ARTICLE INFO

Article history:

Received 24 March 2015

Received in revised form

4 June 2015

Accepted 14 June 2015

Available online 19 June 2015

Keywords:

Rolling contact fatigue

Bearings

Optical microscopy

Electron microscopy

Steel

ABSTRACT

White etching cracks (WECs) have been identified as a main failure mode of wind turbine gearbox bearings (WTGBs). This study reports an investigation of the destructive sectioning of a failed low speed planetary stage WTGB and the damage found at manganese sulphide (MnS) inclusions. The bearing inner raceway was sectioned through its circumferential and axial directions in order to compare the damage around inclusions in different directions. 112 damage initiating inclusions were catalogued and their properties were investigated.

WECs were found attached to MnS inclusions of lengths 3–45 μm at depths of up to 630 μm from the bearing raceway surface and at a wide range of angles of orientation. Damage at MnS inclusions included internal cracking of the inclusions, separation from the surrounding steel matrix, crack initiation and WEC initiation. Evidence has been found to support the theory that WECs are subsurface-initiated by MnS inclusions, but that butterfly cracks with wings propagating at 30–50° from parallel to the raceway surface are not necessarily the same features as MnS inclusion-initiated WECs. Shorter inclusions were found to initiate longer WECs, as were the inclusions that were closer to parallel to the raceway surface in axially sectioned samples.

© 2015 The Authors. Published by Elsevier B.V. This is an open access article under the CC BY license (<http://creativecommons.org/licenses/by/4.0/>).

1. Introduction

The wind industry faces tough challenges to reduce the cost of wind energy; particularly its high operating cost. The European Wind Energy Agency has a planned target of 230 GW of installed wind power capacity by 2020, representing 20% of the total European Union (EU) electricity consumption [1]. This expansion is being limited by a number of maintenance issues, most critically concerning wind turbine gearboxes (WTGs) which are not reaching their anticipated lifespan of 20 years. It is estimated in the United Kingdom that operation and maintenance accounts for 20% of the cost of offshore wind energy [2].

A majority of WTG failures initiate in the wind turbine gearbox bearings (WTGBs) [3], and the exact modes of their failure have been intensively researched and widely investigated by industry. White etching cracks (WEC) have been found to lead to premature failure by white structure flaking (WSF) [4], or axial cracking [5]. Previous work has identified material defects, particularly

manganese sulphide (MnS) inclusions as WEC initiators, in both actual WTGBs obtained from the field and WTGBs after rolling contact fatigue (RCF) testing on large scale test rigs [6–9]. This study will investigate damage initiation at manganese sulphide (MnS) inclusions, by destructively sectioning the inner raceway of a failed planetary stage WTGB. Damaged inclusions were catalogued and their properties were recorded. The objective was to investigate different types of damage caused at the inclusions and to find any links between their properties and possible connections to operating conditions.

1.1. MnS inclusions in bearing steel

MnS inclusions have been classified into three types since 1938 [10]. Type I inclusions are globular in shape and appear in steels with practically no aluminium content. Type II are dendritic chain formations on grain boundaries and appear with the first traces of aluminium (0.005 wt%). Type III are strings of broken silicates and initially appear alongside Type II at levels of 0.01–0.03 wt% aluminium. At levels greater than 0.04 wt%, Type III is the only MnS inclusion to appear [10]. Since typical bearing steel, such as 100Cr6 or 100CrMo7, has a very low aluminium content [11], globular Type I MnS inclusions are most commonly found. MnS inclusions in hot-rolled steels of irregular shape and which are elongated and flattened in the direction of plastic deformation [12] during the

Abbreviations: EU, European Union; SCADA, supervisory control and data acquisition; BCC, body-centred cubic; RCF, rolling contact fatigue; WTG, wind turbine gearbox; WTGB, wind turbine gearbox bearing; WEC, white etching crack; WEA, white etching area; WSF, white structure flaking; MnS, manganese sulphide

* Corresponding author. Tel: +44 114 222 7759; fax: +44 114 222 7890.

E-mail address: h.long@sheffield.ac.uk (H. Long).

metal forming process are randomly distributed. Therefore their orientation may vary from bearing to bearing due to differences in the metal forming process. Inclusions have been observed to have been elongated to different extents in bearing steel and can be defined by their aspect ratio (length/width) when viewed two-dimensionally. Those inclusions with an aspect ratio of less than three are described as globular and those with larger aspect ratios as long and thin [6].

1.2. White etching cracks

Currently, WTGB failure via white etching cracking is not fully understood, despite intense research effort [5,6,9,13–20]; therefore bearing life prediction models have yet to be developed to include this failure mode in the selection of bearings [4,5,16,19]. WECs are physical cracks in the material subsurface decorated by white etching areas (WEAs) and appear white after etching in nital (nitric acid/methanol) solution due to microstructural change that causes the material to be resistant to the etching process [6]. WEAs have been found to be areas of ultrafine nano-recrystallised carbide-free body-centred cubic (BCC) ferrite microstructure [4,18,21]; the WEA microstructure has no, or very few remaining carbides and is supersaturated with dissolved carbon, which makes the material brittle and harder (about 30–50%) than the steel matrix [4,18,22]. Cyclic Hertzian stresses caused by rolling contact at and close to the surface promote the ‘glide’ of subsurface dislocations, which repeatedly interact with retained temper carbides, leading to their dissolution [4,23]. One theory is that when the accumulation of dislocations reaches a critical density; a dislocation cell-like structure forms to release the strain energy [13], possibly explaining why obstacles to dislocation glide, such as inclusions, voids or large carbides have been found to be areas at which WEAs form [21]. This theory is contradicted by findings in [18,24], which suggest that WEAs are formed at “butterfly cracks” by an evolving microstructural change leading to the nanocrystalline structure by material transfer and “rubbing” between inclusions and the steel matrix.

WECs have been observed to form (not necessarily exclusively) from “butterfly cracks”, named such due to their two-dimensional appearance. Despite considerable evidence [6,7,9,15,18,23–26], there has been, as yet, no method devised to prove absolutely that butterflies are indeed the point of damage initiation. Butterflies have been reported to initiate most commonly at inclusions [7,27], but voids and carbides may also be candidates for butterfly initiation [4,5] while other studies have found that voids are most likely to initiate butterflies [28,29]. Impurities may be initiation points due to local Hertzian stress concentration, residual stress from heat treatment, the creation of free surfaces during quenching, and/or dislocation accumulation [7]. WEAs form adjacent to microcracks, or possibly form first and promote microcrack growth. WEAs initiate and propagate between 30–50° and 130–150° from the over-rolling direction, giving the appearance of “butterfly wings”, which may be due to the position of maximum Hertzian unidirectional shear stress [4]. Similar cracks may form in the direction opposite to over-rolling if the rolling direction is reversed [30], or sometimes without this reversal (although the symmetric cracks are smaller than the two formed in the over-rolling direction) [7].

WECs may form irregular crack networks that possibly follow pre-austenite grain boundaries, or may propagate radially from straight-growing cracks [5]. It is claimed by Errichello et al. that through-hardened bearings fail by the axial crack method, whereas carburised bearings with less than 20% retained austenite fail by WSF, based on a comparative metallurgical study of both bearing types [5]. If a network of WECs beneath the contact surface weakens the near-surface material sufficiently, WSF may

occur causing material to flake away from the surface, leading to eventual failure possibly within 1–20% of the L_{10} design life [31–34] predicted by current bearing design standards [35].

1.3. Hertzian stress in RCF line contacts

Using Hertzian line contact theory, it is possible to calculate the approximate depth of maximum unidirectional shear stress τ_{max} , orthogonal shear stress $\tau_{0,max}$, and equivalent (von Mises) stress σ_v . Although this method must be used with some caution, since the contact between rolling element and raceway is neither static nor smooth and is separated by a lubricant film, it is common practise to approximate contact pressures in rolling element bearings using the Hertzian theory [36]. Since in most bearings, both the roller and inner raceway are made from the same material, the standard equation used to calculate the Hertzian contact pressure can be simplified to

$$P_0 = 0.418 \sqrt{\frac{WE}{RL}} \quad (1)$$

where

$$\frac{1}{R} = \frac{1}{r_1} + \frac{1}{r_2} \quad (2)$$

r_1 and r_2 are the radii of the contacting inner raceway and rolling element respectively, W is the contact load (N), L is the width of the raceway, ν and E are Poisson's ratio (0.3) and Young's modulus (210 GPa) of the steel respectively [7]. The width of the contact rectangle, $2b$, is calculated from the contact half-width b , using Eq. (3).

$$b^2 = \frac{4WR}{\pi LE} \quad (3)$$

The position of τ_{max} for line contacts is at $0.78b$, $\tau_{0,max}$, at $0.5b$ and for σ_v , at around $0.7b$. For elliptical contacts between a spherical roller and cylindrical raceway, shear stress maximum depths are as follows: τ_{max} at $0.48a$, $\tau_{0,max}$ at $0.25a$, where a is the radius of the semimajor axis [7,9,37–39].

Grabulov used a RCF loading test rig to apply a contact pressure of 2.6 GPa for 13×10^6 cycles to test specimens with artificial aluminate (Al_2O_3) inclusions, finding that there were three distinct butterfly development zones dependant on depth from the contact surface. At depths of up to 150 μm , fully developed butterflies were found, between 150 and 800 μm , early stages of the butterfly development process had taken place, and at depths deeper than 800 μm , no butterflies were found. For the tested conditions, $\tau_{0,max}$ occurred at a depth of 63 μm and τ_{max} occurred at $\sim 120 \mu m$ (approximate value calculated from position of $\tau_{0,max}$) [39], both values were well within the zone of fully developed butterfly formation. τ_{max} , $\tau_{0,max}$ or a combination of both, may be critical in the formation of WECs.

1.4. MnS inclusions as crack initiation sites

All inclusions may act as crack initiation sites under high enough contact stress [7], however MnS inclusions have been found to be the most likely to interact with WECs in WTGB steel [6,8,25–27]. Shorter inclusions have been found to be more likely to initiate damage than longer inclusions, with the ideal length for crack propagation found to be smaller than 20 μm [6,25]. During quenching, the larger thermal contraction rates of the MnS inclusion than the bulk material, may lead to the detachment of the inclusion from the surrounding bulk material, thereby creating a free surface at the subsurface inclusion [7]. The weak bond between MnS inclusions and the matrix may contribute to the

creation of voids [40] and therefore free surfaces. These free surfaces are potential sites for inclusion separation from the bulk material and for rolling contact fatigue initiated cracking [7]. MnS inclusions that contain oxide parts (for example Al_2O_3) have been found to be more damaging than those which do not contain it because if in contact with the matrix, the oxide part may induce cracking initiating tensile residual stresses [25,27]. Crack orientation has been found to be dependent on the plane of sectioning of a bearing; in the circumferential direction, WECs appear highly radially branched, whereas in the axial direction, WECs often tend to appear more parallel to the raceway axis with less radial crack branching [6].

Although free surfaces around a MnS inclusion may be potential crack initiation sites, it is not necessary for a MnS inclusion to initiate a crack due to the poor bond with the bulk material. A thin, flattened MnS inclusion may itself act as a virtual crack [41] that may propagate into an actual crack. In rail steel, MnS inclusions can become significant crack initiators [42]. It was found that near to the rail surface, all MnS inclusions were deformed first in the strain direction, moved to the shear direction caused by over-rolling, and then flattened as they reached the wear surface. Wear tests on four rail steel types confirmed that almost all deformed MnS inclusions near to the wear surface were associated with cracks [41]. Cracks can be initiated along the highly strain flattened MnS inclusions [43] for a number of reasons: micro-cracks may be initiated at localised bands of deformation in the vicinity of the inclusions [44]; free surfaces may be created in the middle of elongated inclusions due to interfacial debonding and void formation [44]; break up of the inclusions may lead to cracks forming within the inclusion [44], which may go on to propagate into the bulk material [6].

A three-stage process for MnS initiated WEC formation has been hypothesised [22] and is illustrated in Fig. 1, using evidence found in this study. Firstly, the inclusion may fracture along the length of its major axis, as shown in Fig. 1a. Separation of the inclusion from the bulk material may or may not occur. Secondly the crack may propagate into the bulk material surrounding the inclusion, as shown in Fig. 1b,c. Finally, white etching areas (WEAs) may develop along the cracks, shown in Fig. 1d. The evidence from this study was collected at the same time after the WTGB failure thus the order of these events is not certain and the illustrated

process is hypothesised and not confirmed. In this study, WEAs have been found adjacent to separated regions that do not appear to be linked to cracks propagating through the steel matrix, although cracks may exist off the plane of sectioning. It is likely that the WEAs and WECs next to inclusions are different stages of the same process and so this assumption is made throughout this study.

For a “butterfly” to exist at a MnS inclusion, it was found that the inclusion was always cracked in the direction of the major axis [38] and that the inclusions themselves were initiators of cracks/butterflies that propagated to form WECs [6]. Crack initiation at MnS inclusions and the growth of short cracks attached to the inclusions may be explained by Mode I fracture (loading is normal to crack growth direction). Further growth of the cracks is governed by Mode II/III fracture (loading is in-plane shear/off-plane shear) [6,45].

While it is clear from the literature reviewed that MnS inclusions are WEC initiators, it has been found in this study that it is not necessarily the case that they must be cracked along their major axis in order to do so. WEAs may also form at cracks or free surfaces caused by other factors discussed in the above sections. This is investigated in detail in Section 4.

2. Destructive investigation of a failed planetary bearing

A failed bearing from the low speed planetary stage of an onshore wind turbine that was operated in the EU was destructively investigated in order to examine subsurface material damage. The wind turbine gearbox had been operating without major incident for five years. A routine oil analysis was carried out 10 days prior to failure, the subsequent report concluding that wear levels were satisfactory and the routine sampling interval should be maintained. The turbine was taken out of service 10 days later when the supervisory control and data acquisition (SCADA) control system received the low gear oil pressure alarm. After inspection, it was found that the bearing presented in this study, together with other planetary bearings, had catastrophically failed. The operating conditions for this bearing are summarised in Table 1.

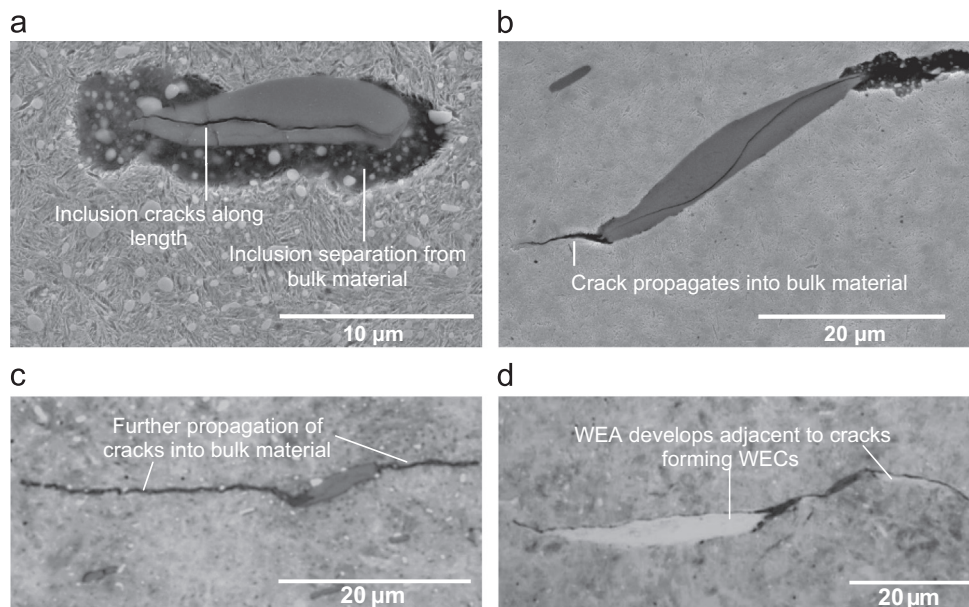


Fig. 1. WEC initiation at MnS inclusions.

Approximate depths of maximum Hertzian stress concentration have been calculated using Eqs. (1)–(3) followed by the approximations listed in Section 1.3 and results are presented in Table 1 based on the bearing dimensions and the recommended maximum contact pressure for planetary WTGBs (1500 MPa) listed in the wind turbine design standard IEC 61400-4 [46], as confirmed in [47].

2.1. Observation of surface damage

Wear was evident for approximately 55% of the inner raceway circumference, but within this region the coverage and type of damage changed. Outside this region there was little to no evidence of wear. The transition from damaged zone to non-damaged zone was immediate and distinct, at a line that is likely to have been positioned at the entry to the loaded zone of the bearing raceway. The variation in damage has been described by three distinct zones as illustrated in Fig. 2.

- **Zone 1:** Non-damaged zone. Over the remaining 45% of the raceway circumference there was very little evidence of damage detectable by eye.
- **Zone 2:** There was a transition to the area of damage coverage. Damage was mainly evident on one side of the raceway towards the non-flanged side of the raceway. The wear damage was intermittent but well defined at a width of around 20 mm for approximately 35% of the raceway circumference. Within the main 20 mm band of damage there was severe macropitting. There were also smaller wear scars outside of this band around the centre of the raceway.
- **Zone 3:** Damage covered most of the raceway width for approximately 20% of the circumference. There was severe macropitting with evidence of material removal from the surface.

Table 1
Operating conditions of failed bearing.

Motion	<ul style="list-style-type: none"> – Nominally rolling contact. – Inner ring stationary with rotational motion of outer ring and cylindrical rollers. – Rotational speed of outer ring: 38 rpm. – Sliding of rolling elements in unloaded zone possible.
Loading	<ul style="list-style-type: none"> – Repeated loading of same inner raceway arc. – Torque reversals and impact loads known to occur. – Misalignment possible. – Bearing contact pressures expected to be approximately 1500 MPa during normal operation [46,47] but may exceed 1700 MPa during WT shutdown [47].
Maximum stress depths	<ul style="list-style-type: none"> – τ_{max} depth: 233 μm – $\sigma_{0,max}$ depth: 150 μm – σ_v depth: 209 μm

From the initial observation of the bearing, it seems clear that the failure occurred at some point in the inner raceway, as the outer raceway was relatively undamaged. The inner raceway was therefore selected for investigation. A total of 40 specimens from the three zones were sectioned, compression mounted in a thermoset resin, ground, polished and etched in 2% nital in methanol solution before observation took place.

2.2. Observation of microstructure

Typical bearing steel is produced by rapid quenching from above the eutectoid temperature, before tempering at around 160 °C, creating a microstructure containing martensite, about 6% volume of retained austenite and 3–4% of cementite particles [7]. From analysing several SEM images such as in Fig. 3 it has been observed that the microstructure is interspersed with spheroidal iron–chromium (M_3C) carbides (cementite), identified as such by their high levels of carbon (C) and chromium (Cr) in Energy Dispersive X-ray Analysis (EDAX) tests. The average chemical composition from a sample of five cementite M_3C carbides with similar appearance to those in Fig. 3 was C 18.1 wt%, Cr 5.3 wt%, and Fe 73.3 wt%. MnS inclusions were present throughout the microstructure and their chemical composition was confirmed using EDAX, an example of which is shown in Fig. 4.

3. Key features of found damage

As previously mentioned, the processes used during the manufacture of bearing raceways, determine the orientation of the MnS inclusions in the steel matrix. In this bearing, inclusions were orientated with their major axis close to parallel with the bearing surface when viewed in an axial cross section as shown in Fig. 5a. They were also elongated to a lesser extent when observed in circumferential sections and were generally angled at approximately 30° from the surface tangent as shown in Fig. 5b. MnS inclusions were consistently orientated in this manner, regardless of their location in the bearing raceway. As a result, it was

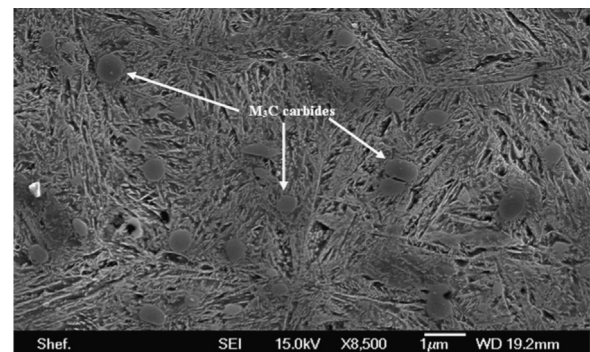


Fig. 3. Bearing steel microstructure highlighting spheroidal iron–chromium (M_3C) carbides.

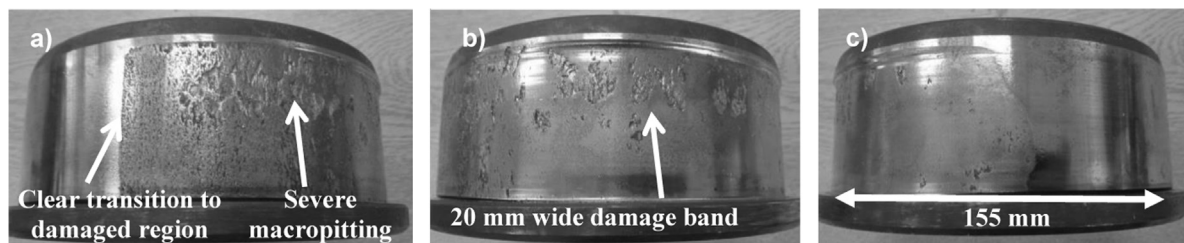


Fig. 2. Photographs of raceway damage (a) Zone 3, (b) Zone 2 and (c) Zone 1.

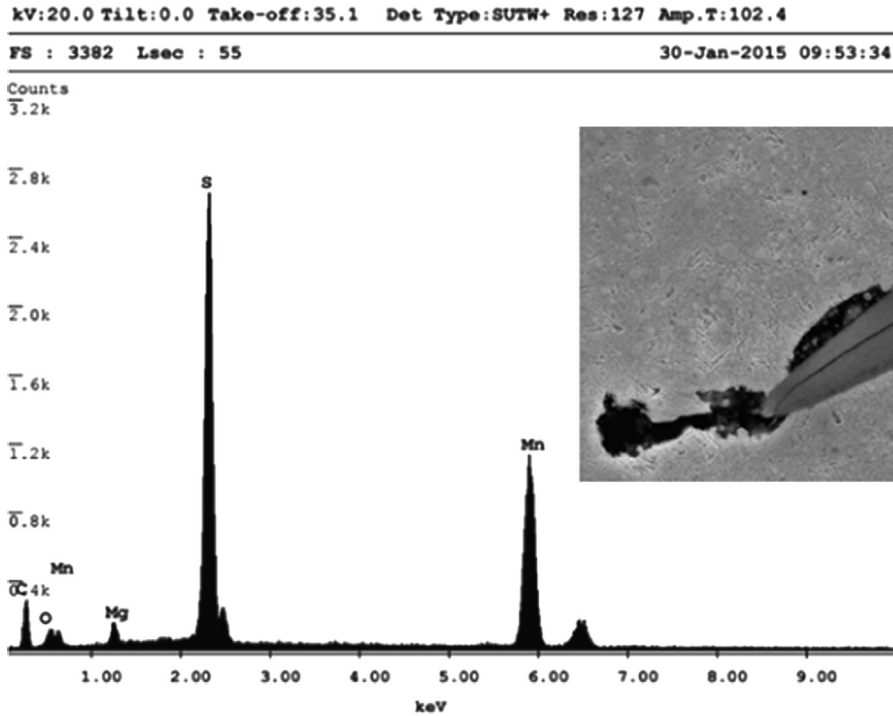


Fig. 4. EDAX spectrum showing chemical composition of MnS inclusion.

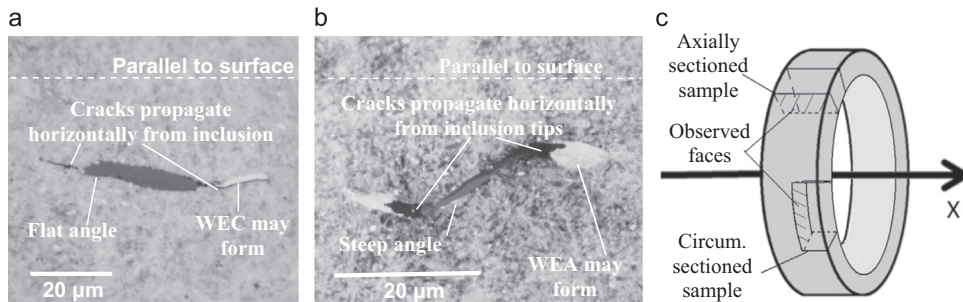


Fig. 5. Inclusion orientation in inner raceway (a) typical MnS inclusion viewed axially, (b) typical MnS inclusion viewed circumferentially and (c) specimen orientation (not to scale).

necessary to prepare specimens sectioned both axially and circumferentially, in order to determine whether cracks form preferentially in either direction. A summary of the specimens investigated and the damage found at each location is provided in Table 2. 112 damage initiating inclusions were found during sectioning and their properties catalogued will be described in Section 4. Inclusion initiated damage included four possible forms: separation of the inclusion from the matrix, internal cracking of the inclusion, crack initiation and propagation from inclusion tip, and WEA formation adjacent to a separated region or a crack (the latter forming a WEC).

3.1. Illustration of undamaged inclusions

Ten MnS inclusions at depths of greater than 5 mm from the contact surface (assumed to be deep enough to be unaffected by the Hertzian stress field) were identified using electron microscopy. These inclusions were found at random within the heavily damaged region, the first 10 being those that were encountered. It was important to do this in order to make distinctions between the damaged inclusions and undamaged inclusions and to ensure that none of the damage was caused by the sectioning process.

Observing the inclusions in Fig. 6 confirms that almost no damage was caused to these deep inclusions, although some black marks are present at the boundary between steel matrix and inclusion. These marks could be small voids caused by separation of the MnS inclusion from the steel matrix during quenching.

3.2. Distinction of “butterfly” and WEC initiating inclusions

It has become apparent that there has been some confusion over the definition of the term “butterfly” in the literature. The term has been used by many to describe both two and four winged features with cracks propagating at 30–50° and 130–150° (close to the angle of maximum unidirectional shear stress) from a central initiating point, usually a void or defect [4,7]. It has also been used to describe short WECs initiated at much shallower or even horizontal angles which, in the opinion of the authors, do not have the same feature. For the remainder of this paper, the term butterfly crack will be used to identify a feature with “wings” propagating at the angles mentioned above and the term “WEC initiating inclusion”, to describe an inclusion with WECs propagating at shallower angles.

Table 2

Summary of sectioned specimens and damage found.

Section details	Sample nos.	Observations/features
Section 1a – circumferential section. Zone 3 damaged region	1–6	– WEC interacting inclusions
Section 3b – axial section. Zone 3 damaged region	6–12	– Crack initiating inclusions – Separation of matrix from inclusions – Butterfly cracks in near surface zone
Section 2a – circumferential section. Zone 1/Zone 2 boundary	13–18	– WEC interacting inclusions
Section 2b – axial section. Zone 1/Zone 2 boundary	19–24	– Crack initiating inclusions – Separation of matrix from inclusions – Butterfly cracks in near surface zone – Significant axial cracking parallel to the raceway (with no attached WEA) – Substantial WEC orientated normal to the raceway surface – Surface initiated cracks by RCF
Section 3a – circumferential section. Zone 2 damaged region	25–30	– WEC interacting inclusions
Section 3b – axial section. Zone 2 damaged region	31–36	– Crack initiating inclusions – Separation of matrix from inclusions – Small butterfly initiated WECs – Large butterfly crack and MnS inclusion interacting WEAs, with WEC propagating to surface – Surface initiated cracks by RCF – Plastically deformed region
Section 4a – circumferential section. Zone 1 non-damaged region	37–40	No evidence of damage

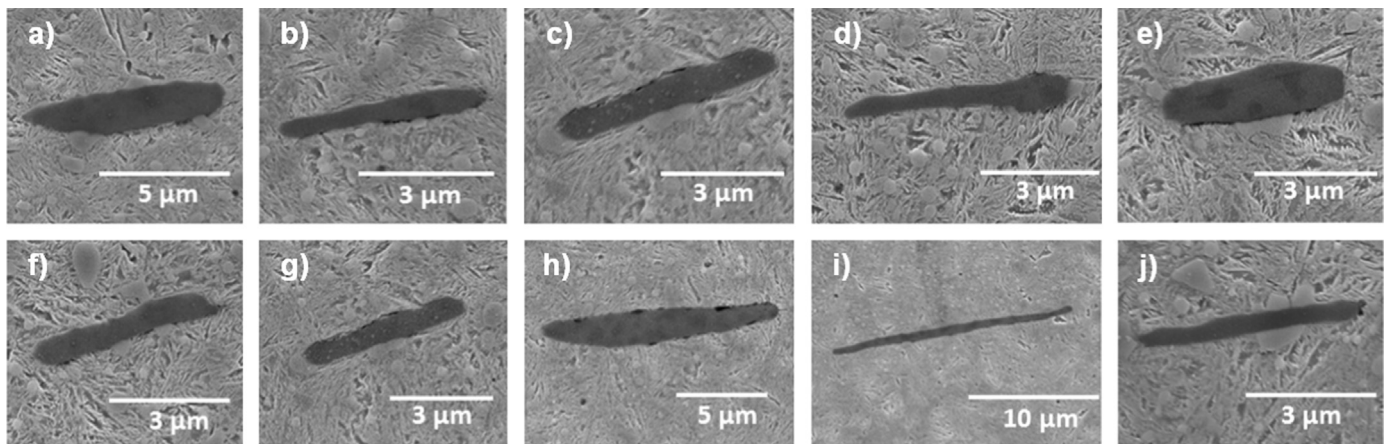
**Fig. 6.** Examples of undamaged inclusions at depths of greater than 5 mm from the raceway surface (specimen 31).

Fig. 7a presents an example of a series of a large butterfly and connected WECs that propagate to the raceway surface. Highly magnified SEM images of the main butterfly feature are presented showing the severe elongation of M_3C carbides in the vicinity of the WEA. Since there was no obvious inclusion initiating any of the WEC features observed in Fig. 7a, approximately $20\ \mu\text{m}$ was ground from the specimen surface before it was polished and etched for observation again. Fig. 7b shows two MnS inclusions that interact with this WEC network, confirming that damage may spread between MnS inclusions and offering evidence that the crack network may have been initiated by MnS inclusions. Fig. 7 is believed to show a late-stage WEC network that may have contributed to the bearing failure; this section will now look in detail at earlier stages of damage, specifically initiating at MnS inclusion.

Of the 112 catalogued inclusions, 89 inclusions (79.5%) were connected to WECs that appeared to have propagated from the inclusion tips. Each of these 89 inclusions had either one or two WECs that tended to propagate at much shallower angles than traditional “butterfly wings” the vast majority at less than 30° from horizontal (discussed further in Section 4). It is suggested

that these MnS inclusion initiated WECs may not be caused by a concentration of unidirectional shear stress as “butterfly wings” are thought to be [4,6–9,38], but are initiated due to mode I loading of the inclusion tips at locations near to the maximum equivalent stress, which would explain their near parallel-to-surface propagation. Examples of these inclusion-initiated WECs are shown in Fig. 8a–w, which were taken from circumferentially sectioned specimens. Fig. 8a,b is SEM images thus it cannot be proved from the images that the highlighted WEA regions are indeed white in colour. It seems however, that by the given evidence presented in Fig. 8c–w, it can be ascertained that these regions are WEAs. It can be clearly seen that the angle of WEC propagation in all example images (with the possible exception of Fig. 8l and q) is lower than the angle of butterfly wing propagation presented in Fig. 7. This finding is in line with the findings presented in [48], which states that the most common angle of WEC propagation in bearing steel is between -10° and $+20^\circ$ from the horizontal, where the sign indicates an angle below or above the horizontal.

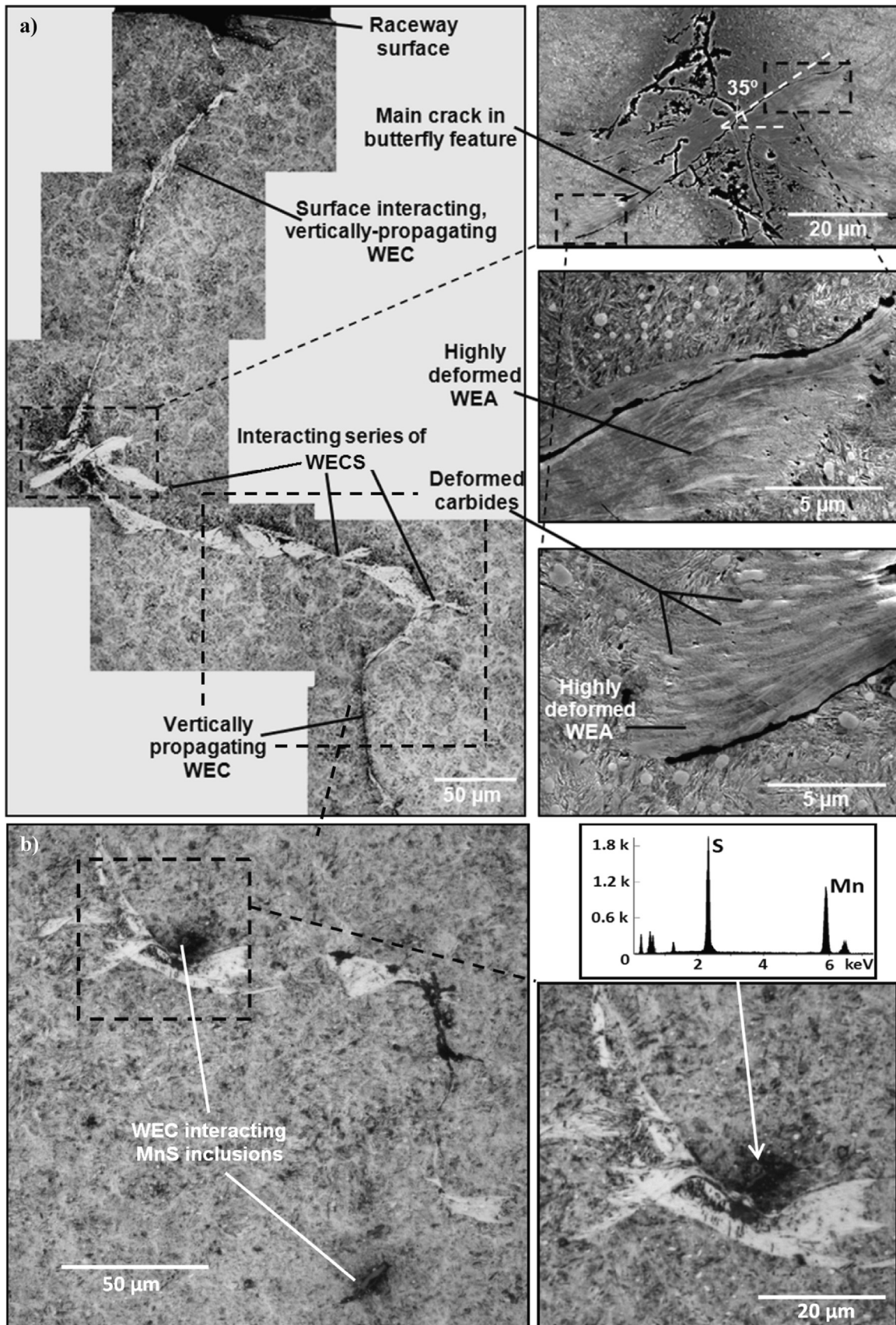


Fig. 7. Series of butterflies and connected WECs in circumferential section (a) first section observed and (b) second section observed approximately 20 μm below the first section.

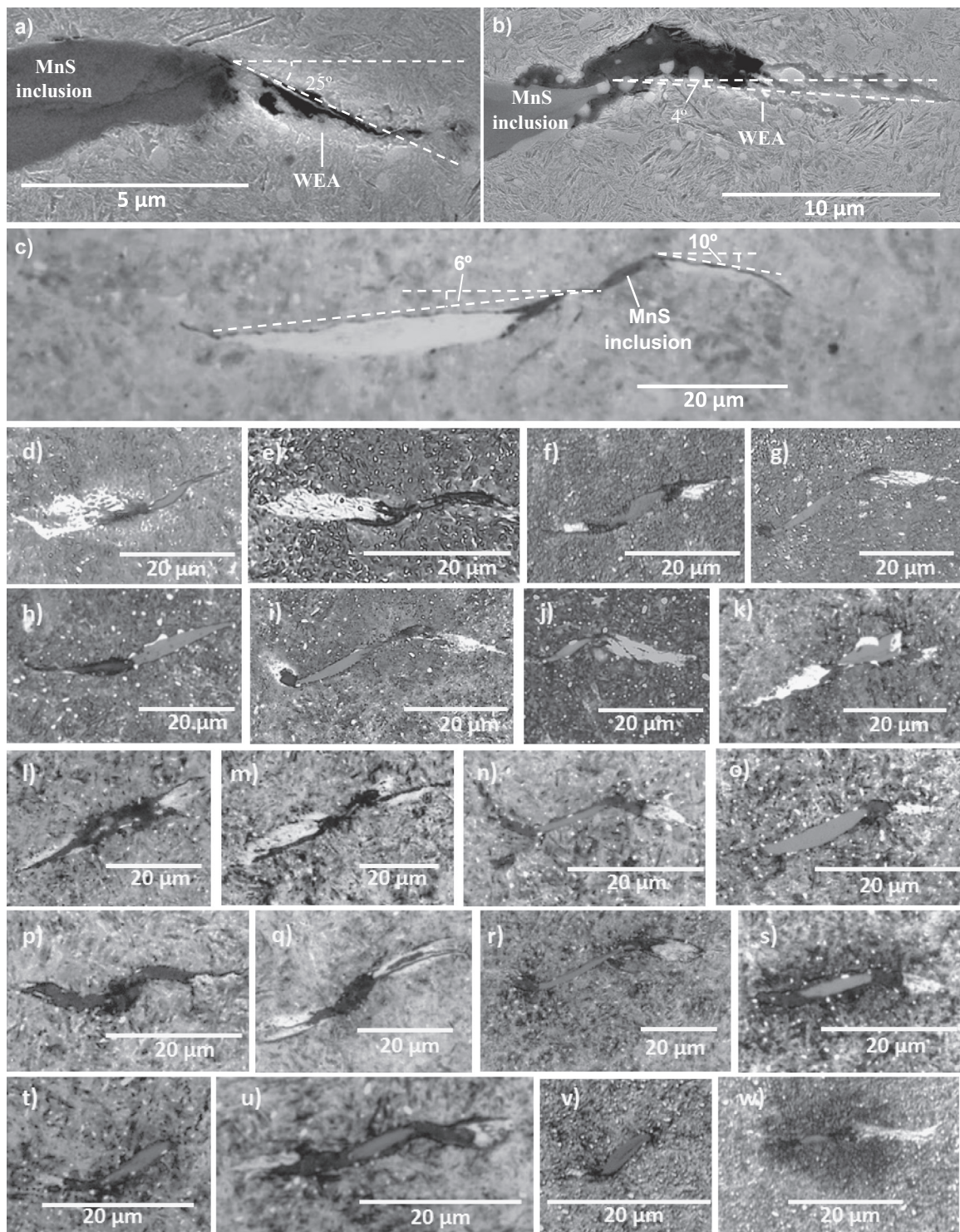


Fig. 8. Examples of WEC initiating MnS inclusions (circumferentially sectioned specimens).

3.3. Subsurface inclusion-initiated WECs

There is debate regarding the location of WEC initiation; broadly there are two arguments:

1. WECs initiate subsurface and propagate up to the surface, leading to failure, either by WSF or axial cracking [4,6,7,16–18,20,31,49].
2. WECs initiate on the surface and propagate downwards [22], meaning that they are a result of surface failure rather than its

cause.

Argument 1 and argument 2 are not necessarily mutually exclusive; however, evidence found in this study certainly suggests that argument 1 is correct and that WECs may initiate subsurface, most commonly at MnS inclusions. The evidence presented in Fig. 8 supports argument 1 and Fig. 9 presents further evidence that cracks and WECs are initiated at MnS inclusions. Fig. 7 shows that MnS inclusions and butterflies interact with WECs, which supports argument 1, although does not offer proof that the

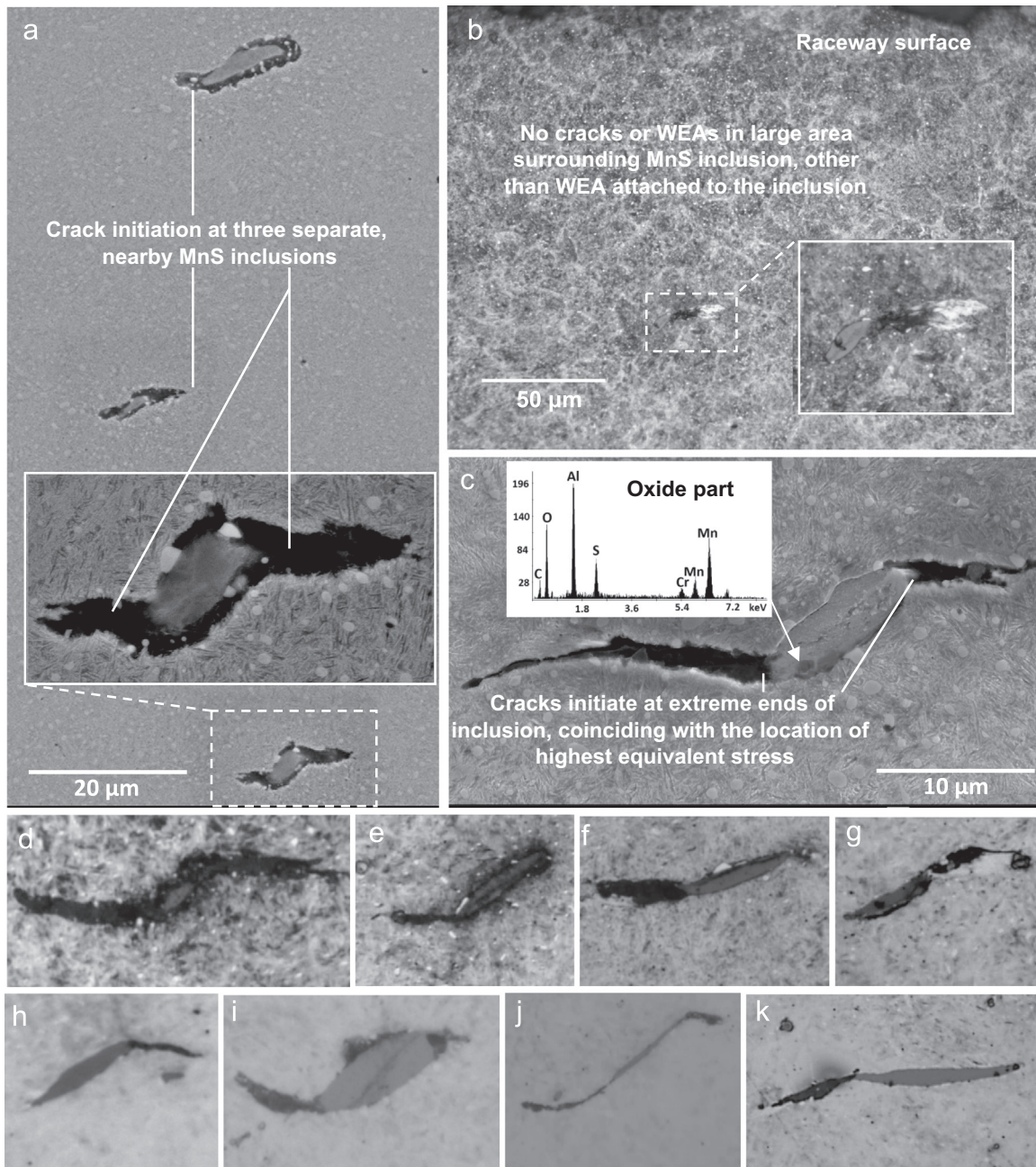


Fig. 9. Evidence supporting crack and WEC initiation at MnS inclusions.

damage was initiated from the butterfly or from the inclusions. Fig. 9a shows three nearby inclusions, which have each independently initiated cracking. They are not part of an extended crack network and no other cracks are visible on this plane, therefore crack initiation must have begun at the inclusions. Fig. 9b shows a typical WEA, initiated at an inclusion, around 150 μm below the raceway surface. Again the feature does not appear to be linked to any extended crack network. Since all 112 catalogued damage initiating inclusions did not appear to be part of a larger crack network, the evidence that the damage was initiated at the inclusions is conclusive. Fig. 9c (SEM) and Fig. 9d–k (optical) show typical separation and cracks formed at the ends of damaged inclusions. The SEM image shows an EDAX reading of a darker part of the inclusion near to the cracks, revealing it to be an area of Al_2O_3 oxide, which may have influenced WEC initiation. Studies have found that MnS inclusions containing oxide parts are more damaging than those that do not contain the oxide parts [25,27],

however no evidence suggesting that oxide parts are required for WECs initiation was found in this study. Every WEC found in this study appeared to have initiated at the inclusion tips (the lowest radius of curvature), coinciding with the location of maximum stress concentration around the inclusion [50–52].

It could be the case that WECs remain close to the initiating inclusion and never propagate to significant distances through the material. Fig. 7b however, provides evidence that WECs may propagate between MnS inclusions and affect greater areas, although it cannot be considered conclusive because the WEC may have approached the vicinity of the highlighted inclusions randomly. It should also be noted that it is possible that any separation around inclusions shown in Figs. 7–11 may have been exaggerated in some images due to the etching process; since etchant may not be washed out completely from the small voids/separated regions between inclusion and matrix, causing acid damage.

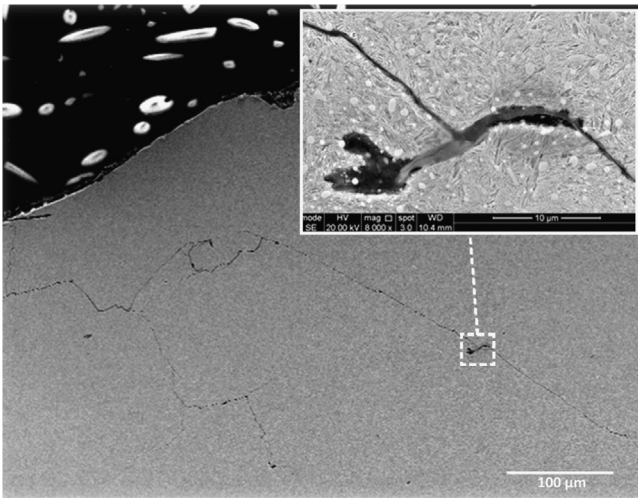


Fig. 10. Crack “deflection” by MnS inclusion.

It has been reported [53] that MnS inclusions themselves may act as “virtual cracks”, which may propagate actual cracks due to their low strength. An example of a MnS inclusion acting as a virtual crack is presented in Fig. 10, where the inclusion that is intersected by a large crack network (assumed to be surface initiated with no apparent attached WEA), diverts a crack by a distance of approximately 10 μm . This was a rare occurrence based on the observations in this study, since this was the only example of such an interaction. However, the finding supports the theory that cracks preferentially propagate along MnS inclusions, rather than the surrounding matrix and shows that they are a “weak spot” within the steel microstructure.

3.4. Damage initiation and propagation at MnS inclusions

The observed damage at MnS inclusions found during sectioning is summarised in detail in Fig. 11. Inclusions are initially undamaged and well-bonded to the matrix (stage 0). The first sign of damage may be internal cracking of the inclusion (stage 1a) and/or separation of the inclusion from the steel matrix (stage 1b). Cracking may be initiated into the steel matrix due to Mode I loading [6,45] (stage 2), possibly from propagation of the stage 1a internal crack, from stage 1b type separation, or from the inclusion tip that may act as a stress concentration point. WEAs then form at stage 1b separation (stage 3a) or, at stage 2 type propagated cracks due to Mode II/III loading [6,45] (stage 3b). Further propagation of cracks and sometimes, of their attached WEAs may then take place (stage 4), leading to the propagation of WECs, far away from the MnS inclusions. The likelihood of each damage type occurring and the possible relationships between each are investigated in Section 4.

4. Analysis of inclusion properties

112 damage initiating inclusions from circumferentially and axially sectioned samples were identified and catalogued. The following data was recorded, with the aim of finding trends between the different properties. This section discusses links between the following inclusion properties and damage types found:

- Depth of inclusion from surface.
- Angle of inclusion.
- Whether the inclusion is internally cracked.
- Whether the inclusion is separated from the surrounding steel

matrix.

- Total length of crack initiated from inclusion (left side crack length + right side crack length).
- Total length of WEC initiated from inclusion (left side crack length + right side crack length).

4.1. Relationship between damage types at MnS inclusions

Fig. 12 shows the relationship between three types or stages of damage at MnS inclusions; internal cracking, separation from the bulk material and WECs linked to the inclusions. Fig. 12a shows that 29% of damaged inclusions were both internally cracked and WEC initiating, while, 50% had initiated WECs without being internally cracked. This result clearly demonstrates that an inclusion does not necessarily need to be internally cracked in order to initiate a WEC. Similar percentages in Fig. 12b show that separation from the bulk material has a similar link to the probability of the inclusion interacting with a WEC, with 28% of separated inclusions being linked to WECs, and 51% of non-separated being also linked. This shows that an inclusion that does not separate from the steel matrix is more likely to initiate a WEC than one that does, perhaps because some stress is relieved by the separation. Fig. 12c appears to show no strong prevalence of damage occurring at inclusions that are internally cracked or that are separated from the bulk material, or those that are both internally cracked and separated.

4.2. Variation of MnS inclusion initiated damage with depth

No trends were found when comparing the angle and the size of inclusions with their depth from the raceway surface, thus it is clear that inclusion distribution is random in the sample bearings and that the effects of over-rolling during service have little influence on the size and orientation of the inclusions. In addition, WECs were found on many of the deepest damaged inclusions, to a depth of approximately 600 μm from the raceway surface (corresponding to a contact stress of around 2.6 GPa if τ_{max} occurred at that depth, possibly suggesting that the bearing may have experienced extremely high loading). It was interesting, however, that no internally cracked or separated inclusions were found deeper than 430 μm . In fact the mean depths for inclusions that were internally cracked and for those that had separated from the surrounded bulk material were just 3 μm different (mean values of 219.5 μm and 216.2 μm respectively). This suggests that inclusion cracking and inclusion separation may be affected by similar initiation mechanisms. These results are outlined in Fig. 13.

The mean depths of damaged inclusions that were cracked, separated, or had initiated WECs were all very close to the position of calculated values of τ_{max} and σ_v (from Table 1). This finding is similar to that of Grabulov [18] as discussed in Section 1.4. The mean values did not correspond as closely to the depth of $\tau_{0,max}$, which suggests that it may not be as critical as τ_{max} and σ_v for WEC initiation at MnS inclusions. Grabulov found that $\tau_{0,max}$ was critical for butterflies as Al_2O_3 inclusions, again suggesting that these features are not the same. Fig. 14 displays the mean and maximum crack lengths at inclusions within different ranges of depths in (a) circumferentially and (b) axially sectioned specimens. It can be seen that the mean value of WEC lengths is relatively constant, about 10 μm , in the circumferentially sectioned specimens, up to a depth of 500 μm . While WEC length is greatest between 200 and 300 μm in depth in axially sectioned specimens (with the exception of the one inclusion found in the range 400–500 μm), which are corresponding with the depths of τ_{max} and σ_v .

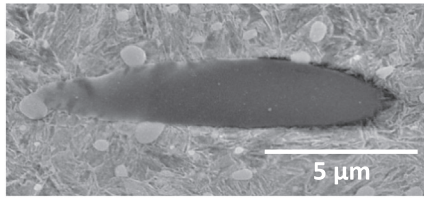
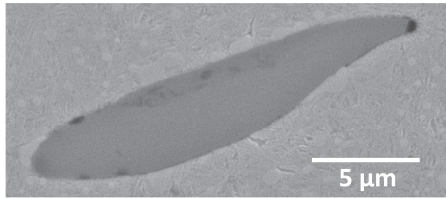
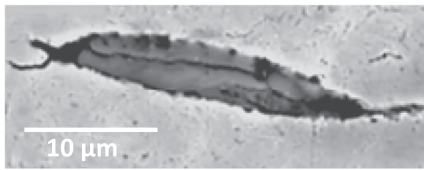
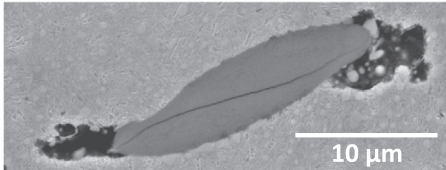
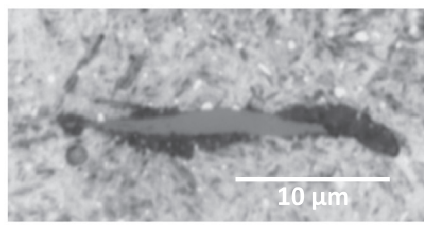
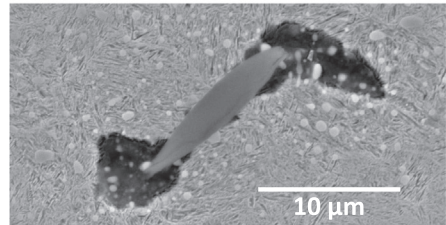
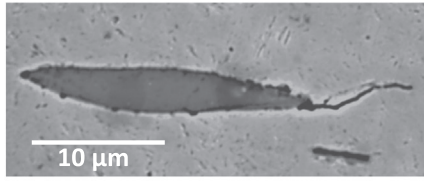
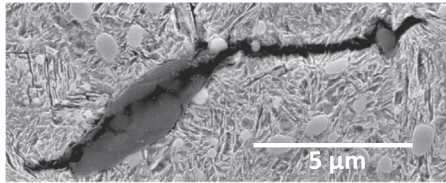
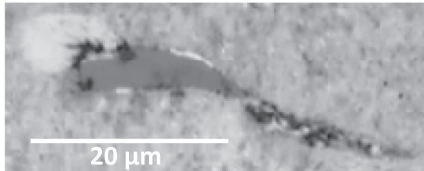
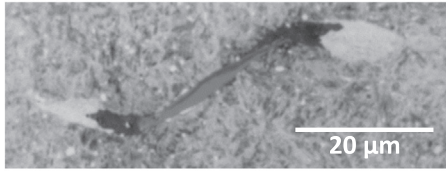
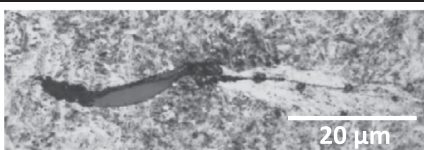

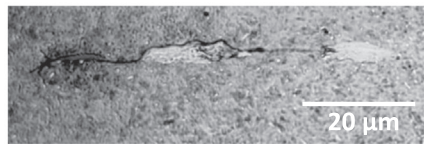
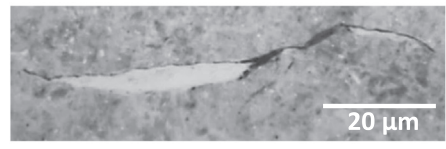
	Axial cross-section shape	Circumferential cross-section
Stage 0 Undamaged inclusion		
Stage 1a Inclusion internal cracking		
Stage 1b Separation of inclusion from matrix		
Stage 2 Crack propagation into matrix from inclusion tip		
Stage 3a WEA propagates from separation at inclusion tips		
Stage 3b WEA develops adjacent to cracks forming WEC		
Stage 4 Further propagation of crack and WEC into bulk material		

Fig. 11. Damage initiation and propagation at MnS inclusions.

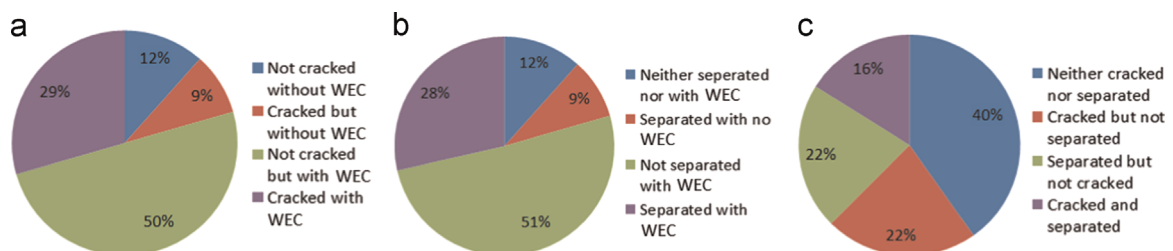


Fig. 12. Relationship between damage types: (a) internal cracking and WEC formation, (b) separation from matrix and WEC formation and (c) internal cracking and separation from bulk material.

4.3. Variation of WEC length with MnS inclusion orientation angle

No trends were found when WEC lengths were compared to inclusion orientation in the circumferential sectioned samples, however Fig. 15a shows that mean WEC lengths were generally shorter at the extreme ends of the orientation angle range (i.e. angles $> 10^\circ$ and $< 60^\circ$). Fig. 15b shows that the length of cracks propagating in the axial direction were generally longer in “flatter” axially sectioned inclusions. That is to say, that it appears, that the closer the inclusion's major axis is to being parallel with the bearing raceway surface, the longer the initiated propagated crack is likely to be. The direction of the inclusion orientation from parallel (anticlockwise or clockwise) is not considered since the stress field is symmetric when viewed on the axial section (assuming no misalignment).

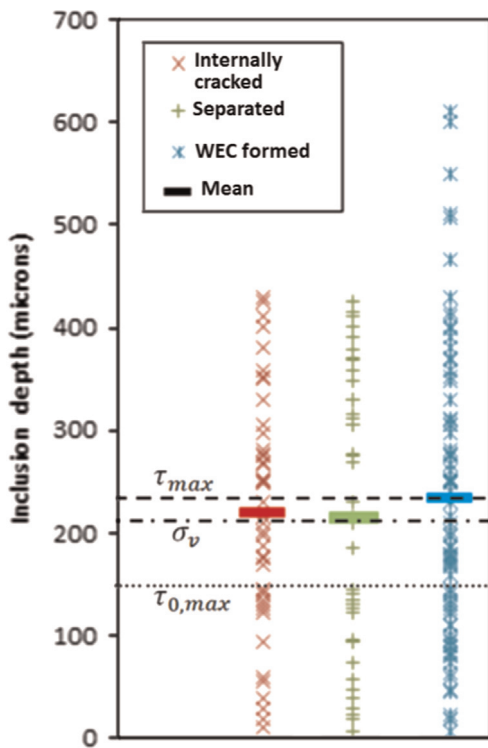


Fig. 13. Variation of inclusion initiated damage with inclusion depth and depths of maximum stresses τ_{max} , $\tau_{0,max}$ and σ_v .

4.4. Variation of WEC length with MnS inclusion length

Clear trends were found between the length of WECs propagating into the bulk material and the length of the initiating MnS inclusions. As shown in Fig. 16, crack length tended to be longer at smaller inclusions for both axially and circumferentially sectioned samples (ignoring the single inclusion found that was less than $8 \mu\text{m}$ in length). A study at the University of Southampton in which a WTGB was similarly sectioned found that smaller inclusions (average length less than $20 \mu\text{m}$) were the most likely to initiate WECs [6,25], although this contradicts the findings presented in [54], which states that coarser inclusion sizes, in general, have a larger local stress-concentration factor. The highest mean value of WEC lengths for both circumferentially and axially sectioned specimens was initiated by inclusions of lengths between 8 and $16 \mu\text{m}$. The downward trend is clear in both Fig. 16a and b. The results in Figs. 14–16 also show that WECs tended to be longer in axially sectioned inclusions than circumferentially sectioned inclusions, suggesting that WECs preferentially propagate in the axial direction, perhaps explaining why through-hardened bearings have been found to fail via axial cracking [5].

5. Conclusions

By investigating a failed wind turbine gearbox bearing, MnS inclusions were found to have initiated significant levels of damage to the subsurface of an inner raceway of a planetary bearing in a wind turbine gearbox. By observing and cataloguing the damage, the following conclusions were drawn up:

1. In the failed WTGB investigation, WECs were preferentially initiated at MnS inclusions ahead of other inclusion types. Four main forms of damage were found at MnS inclusions: internal cracking, crack propagation into the bulk material without an attached WEA, separation from the surrounding material and WEC initiation.
2. The mean depth of MnS inclusions that had initiated WECs in the subsurface of the analysed WTGBs interacted very strongly with the positions of maximum equivalent stress and maximum unidirectional shear stress. Since the majority of the 89 WEC initiating MnS inclusions (79.5% of catalogued inclusions) had WECs that propagate at shallower angles than traditional “butterfly wings”, it is hypothesised that the WECs may have been initiated due to stress concentrations at inclusion tips at locations near to the maximum equivalent stress.
3. It was found to be more likely for a WEC to form at an inclusion that was not internally cracked (50% of catalogued inclusions),

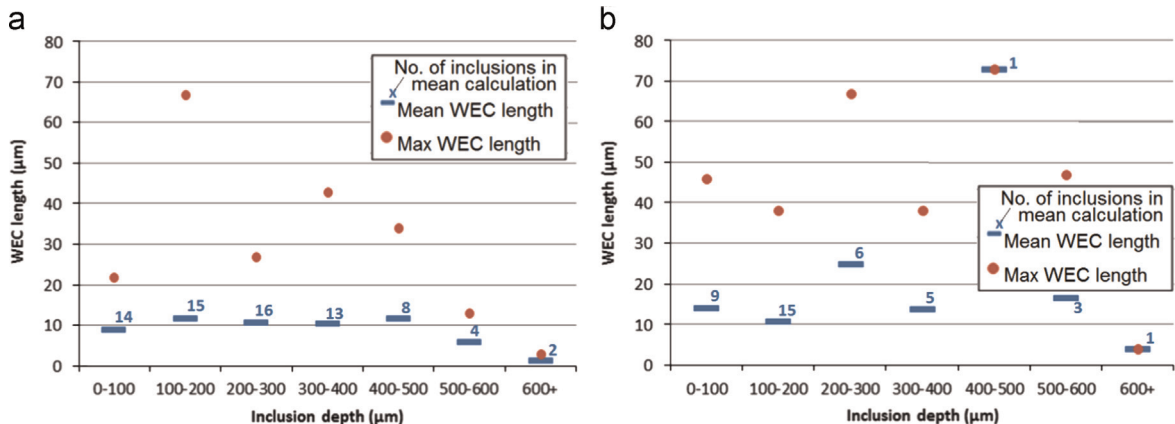


Fig. 14. Variation of mean and max WEC length with MnS inclusion depth in (a) circumferentially sectioned specimens, and (b) axially sectioned specimens.

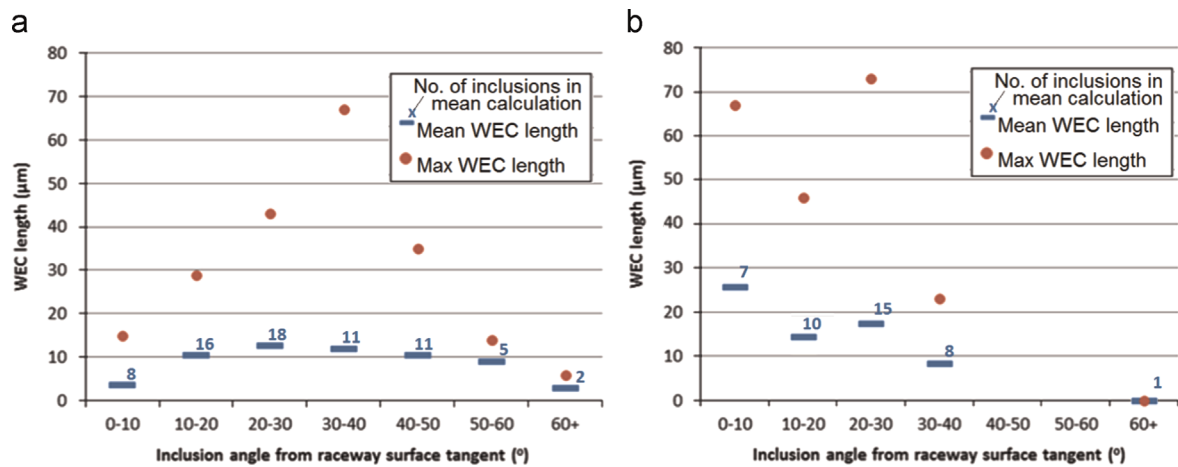


Fig. 15. Variation of mean and max WEC length with MnS inclusion orientation angle in (a) circumferentially sectioned specimens, and (b) axially sectioned specimens.

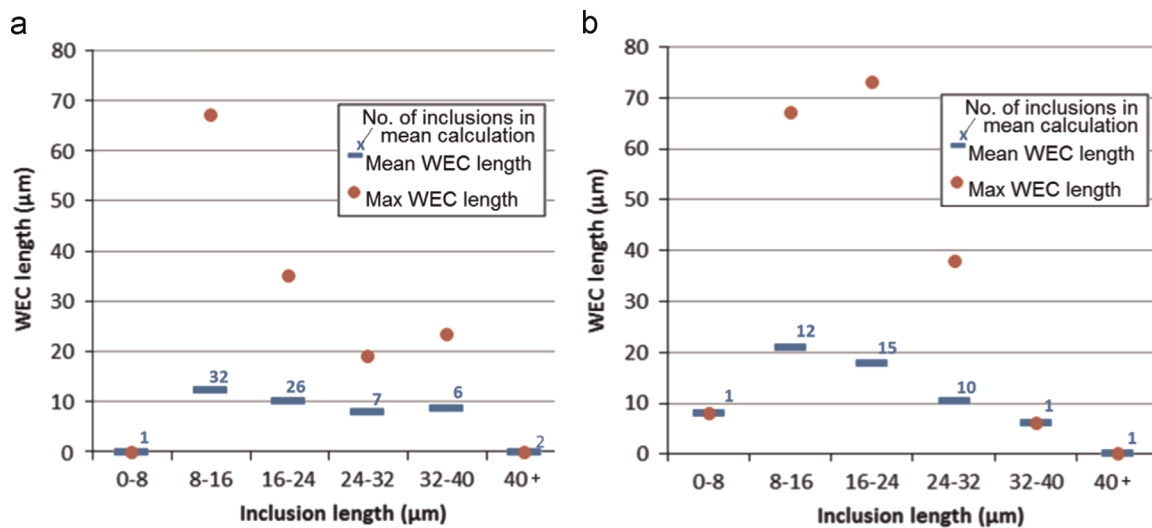


Fig. 16. Variation of mean and max WEC length with MnS inclusion length in (a) circumferentially sectioned specimens, and (b) axially sectioned specimens.

than one that was internally cracked (29% of catalogued inclusions). It was found to be more likely for a WEC to form at an inclusion that was not separated from the surrounding material (51% of catalogued inclusions), than one that was separated (28% of catalogued inclusion).

- Neither internal cracking of inclusions nor separation of inclusions from the surrounding material occurred at inclusions deeper than $\sim 420 \mu\text{m}$ from the raceway surface, although WECs were found at inclusions as deep as $\sim 630 \mu\text{m}$.
- Cracks propagating from inclusions tended to be longest when initiated by smaller inclusions of around the mean value of 8–16 μm in length. When viewed in an axial cross-section, longer WECs were found to have initiated from inclusions that were closer to being parallel with the raceway surface, than those that were more steeply angled. In general, cracking was more extensive in the axial direction than circumferential direction, although damage propagated significantly in both directions.

Ricardo for funding this research and our anonymous partner for the provision of the failed bearing.

References

- [1] European Wind Energy Agency, The European Wind Initiative 2013 [online]. Available: (<http://www.ewea.org/publications/reports/the-european-wind-initiative-2013>), 2010.
- [2] Innovation Coordination Group Technology Innovation Need Assessment (TINA), Offshore Wind Power Summary Report Carbon Trust, 2012.
- [3] W. Musial, S. Butterfield, B. McNiff, Improving wind turbine gearbox reliability, Conference Paper, National Renewable Energy Laboratory, NREL/CP-500-41548, 2007.
- [4] M. -H. Evans, White structure flaking (WSF) in wind turbine gearbox bearings: effects of 'butterflies' and white etching cracks (WEC), Mater. Sci. Technol. 28 (1) (2012) 3–22.
- [5] R. Errichello, R. Budny, R. Eckert, Investigations of bearing failures associated with white etching areas (WEAs) in wind turbine gearboxes, Tribol. Trans. 56 (6) (2013) 1069–1076.
- [6] M. -H. Evans, A. Richardson, L. Wang, R.J.K. Wood, Serial sectioning investigation of butterfly and white etching crack (WECs) formation in wind turbine gearbox bearings, Wear 302 (1–2) (2013) 1573–1582.
- [7] H. Bhadeshia, Steels for bearings, Prog. Mater. Sci. 57 (2012) 268–435.
- [8] T.B. Lund, Sub-surface initiated rolling contact fatigue – influence of non-metallic inclusions, processing history, and operating conditions, J. ASTM Int. 7 (2010) JA102559.
- [9] R.D.C. Arnaud, Tribological analysis of white etching crack (WEC) failures in rolling element bearings (Doctoral thesis), INSA Lyon, 2014.

Acknowledgements

The authors would like to thank United Kingdom EPSRC Doctoral Training Grant (EP/J 500525/1 and EP/K 503149/1) and

- [10] C.E. Sims, F.B. Dahle, Effect of aluminium on the properties of medium carbon cast steel, *AFS Trans.* 46 (1938) 65.
- [11] British Standards Institution, Wrought steels for mechanical and allied engineering purposes. Requirements for carbon, carbon manganese and alloy hot worked or cold finished steels, PD 970:2005, 2005.
- [12] L.H. Hihara, R.P. Adler, R.M. Latanision, *Environmental Degradation of Advanced and Traditional Engineering Materials*, CRC Press, Boca Raton, FL (2013), p. 2013.
- [13] K. Iso, A. Yokouchi, H. Takemura, Research Work for Clarifying the Mechanism of White Structure Flaking and Extending the Life of Bearings, SAE, 2005.
- [14] B. McNiff, Wind Turbine Gearbox Reliability in Sandia National Laboratories Wind Turbine Gearbox Reliability Workshop, Albuquerque, NM, 2006.
- [15] M.-H. Evans, J.C. Walker, C. Ma, L. Wang, R.J.K. Wood, FIB/TEM study of butterfly crack formation and white etching area (WEA) microstructural changes under rolling contact fatigue in 100Cr6 bearing steel, *Mater. Sci. Eng. A* 570 (2013) 127–134.
- [16] M.N. Kozalas, G.L. Doll, Tribological advancements for reliable wind turbine performance, *Philos. Trans. R. Soc. A* 368 (2010) 4829–4850.
- [17] J. Gegner, W. Nierlich, The Bearing Axial Cracks Root Cause Hypothesis of Frictional Surface Crack Initiation and Corrosion Fatigue Driven Crack Growth [online]. Available: (http://www.nrel.gov/wind/pdfs/day2_sessioniv_2_skf_gegner.pdf), 2011.
- [18] A. Grabulov, U. Ziese, H.W. Zandbergen, TEM/SEM investigation of microstructural changes within the white etching area under rolling contact fatigue and 3-D crack reconstruction by focused ion beam, *Scr. Mater.* 57 (7) (2007) 635–638.
- [19] J. Luyckx, WEC failure mode on roller bearings, Presentation at Wind Turbine Tribology Seminar, Hansen Transmissions, 2011.
- [20] H. Uyama, H. Yamada, H. Hidaka, N. Mitamura, The effects of hydrogen on microstructural change and surface originated flaking in rolling contact fatigue, *Tribol. Online* 6 (2) (2011) 123–132.
- [21] P. Becker, Microstructural changes around non-metallic inclusions caused by rolling contact fatigue of bearing steels, *Met. Technol.* 8 (1) (1981) 234–243 1981.
- [22] J. Gegner, Tribological Aspects of Rolling Bearing Failures, InTech, Europe (2011), p. 33–94.
- [23] A. Vincent, G. Lormand, P. Lamagnere, L. Gosset, D. Girodin, G. Dudragne, R. Fougères, From white etching areas around inclusions to crack nucleation in bearing steels under rolling contact fatigue, in: *Bearing Steels: Into the 21st Century*, ASTM International, West Conshohocken, PA, 1998, pp. 109–123.
- [24] A. Grabulov, R. Petrov, H.W. Zandbergen, EBSD investigation of the crack initiation and TEM/FIB analyses of the microstructural changes around the cracks formed under Rolling Contact Fatigue (RCF), *Int. J. Fatigue* 32 (3) (2010) 576–583.
- [25] M.-H. Evans, L. Wang, H. Jones, R.J.K. Wood, White etching crack (WEC) investigation by serial sectioning, focused ion beam and 3-D crack modelling, *Tribol. Int.* 65 (2013) 146–160.
- [26] M. Brueckner, J. Gegner, A. Grabulov, W. Nierlich, J. Slycke, Alternative butterfly formation mechanisms in rolling contact fatigue, in: *Proceedings of the 5th International Conference on 'Very High Cycle Fatigue'*, Berlin, 2011.
- [27] M.-H. Evans, A.D. Richardson, L. Wang, R.J.K. Wood, Effect of hydrogen on butterfly and white etching crack (WEC) formation under rolling contact fatigue (RCF), *Wear* 306 (1–2) (2013) 226–241.
- [28] M. Selecká, A. Šalák, Durability and failure of powder forged rolling bearing rings, *Wear* 236 (1999) 47–54.
- [29] V. Pasarić, J. Croitoru, S. Constantinescu, E. Dobrescu, E. Cioaca, The origin and content of Al₂O₃ nonmetallic inclusions in ball bearing steel, *Metalurgia* 33 (1981) 329–349.
- [30] R. Tricot, J. Monnot, M. Lluansi, How microstructural alterations affect fatigue properties of 52100 steel, *Met. Eng. Q.* 12 (1972) 39–47.
- [31] A. Greco, S. Sheng, J. Keller, A. Eridemir, Material wear and fatigue in wind turbine systems, *Wear* 302 (1–2) (2013) 1583–1591.
- [32] K. Ihata, T. Shiga, A. Umeda, Rolling Bearing Assembly Having Magnet to Prevent Brittle Flaking, Denso Corporation, USA, 2009.
- [33] S. Tanaka, N. Mitamura, Y. Murakami, Influence of sliding and chromium content in the steel on the white structural change under rolling contact, in: *Proceedings of Global Powertrain Conference*, Dearborn, MI, 2004.
- [34] J. Luyckx, W. Broeders, J. Geertsom, Method for increasing the fatigue strength of a predominantly steel mechanical part of a wind turbine and/or for reducing the tendency to form what are called “white etching cracks” or “brittle flakes” in such steel mechanical parts, Hansen Transmissions International, USA, 2009.
- [35] International Organization for Standardization, BS ISO 281: Dynamic load ratings and rating life, 2007.
- [36] G.W. Stachowiak, A.W. Batchelor, *Engineering Tribology*, Elsevier, Oxford, 2005.
- [37] G. Fajdiga, Computational fatigue analysis of contacting mechanical elements, *Teh. Vjesn.* 22 (1) (2015) 169–175.
- [38] M.-H. Evans, White structure flaking failure in bearings under rolling contact fatigue (Doctoral thesis), University of Southampton, 2013.
- [39] A. Grabulov, Fundamentals of rolling contact fatigue (Doctoral thesis), University of Belgrade, Serbia, 2010.
- [40] L.d.C.F. Canale, G.E. Totten, R.A. Mesquita, Failure Analysis of Heat Treated Steel Components, ASM International, U.S., 2008.
- [41] A.J. Perez-Unzueta, J.H. Beynon, Microstructure and wear resistance of pearlitic rail steels, *Wear* 162–164 (Part A) (1993) 173–182.
- [42] S.K. Dhua, R. Amitava, S.K. Sen, M.S. Prasad, K.B. Mishra, S. Jha, Influence of nonmetallic inclusion characteristics on the mechanical properties of rail steel, *J. Mater. Eng. Perform.* 9 (6) (2000) 700–709.
- [43] C. Liu, M. Bassim, S. Lawrence, Evaluation of fatigue-crack initiation at inclusions in fully pearlitic steels, *Mater. Sci. Eng.* 167 (1–2) (1993) 108–113.
- [44] A. Chard, Deformation of inclusions in rail steel due to rolling contact (Doctoral thesis), University of Birmingham, England, 2011.
- [45] M. Lewis, B. Tomkins, A fracture mechanics interpretation of rolling bearing fatigue, *Proc. Inst. Mech. Eng. Part J – J. Eng.* 226 (5) (2012) 389–485.
- [46] International Organisation for Standardization, IEC 61400-4:2012: Wind turbines-Part 4: Design requirements for wind turbine gearboxes, 2012.
- [47] T. Bruce, H. Long, R.S. Dwyer-Joyce, Dynamic modelling of wind turbine gearbox bearing loading during transient events, *IET Renew. Power Gener.* (2015), <http://dx.doi.org/10.1049/iet-rpg.2014.0194> 10pp, in press.
- [48] J.-H. Kanga, R.H. Vegter, P.E.J. Rivera-Diaz-del-Castillo, Rolling Contact Fatigue in Martensitic 100Cr6: Subsurface Hardening and Crack Formation, SKF University Technology Centre, Cambridge (2014), p. 2014.
- [49] R.H. Vegter, J.T. Slycke, The role of hydrogen on rolling contact fatigue response of rolling element bearings, *J. ASTM Int.* 7 (2009) 1–12.
- [50] M.S. Joo, D.-W. Suh, H.K.D.H. Bhadeshia, Mechanical anisotropy in steels for pipelines, *ISIJ Int.* 53 (2013) 1305–1314.
- [51] D. Radaj, M. Vormwald, *Advanced Methods of Fatigue Assessment*, Springer, Berlin, 2012.
- [52] Y. Murakami, *Metal Fatigue: Effects of Small Defects and Nonmetallic Inclusions*, Elsevier, Oxford, 2002.
- [53] C. Luo, Modeling the behavior of inclusions in plastic deformation of steels (Doctoral thesis), Royal Institute of Technology, Sweden, 2001.
- [54] S. Mackenzie, Overview of the Mechanisms of Failure in Heat Treated Steel Components in Failure Analysis of Heat Treated Steel Components, ASM International, Materials Park (2008), p. 43–86.